The following publication Wang, Q., Shi, W., Atkinson, P. M., & Wei, Q. (2016). Approximate area-to-point regression kriging for fast hyperspectral image sharpening. IEEE Journal of Selected Topics in Applied Earth Observations and Remote Sensing, 10(1), 286-295 is available at https://doi.org/10.1109/JSTARS.2016.2569480.

Approximate Area-to-Point Regression Kriging for Fast Hyperspectral Image Sharpening

Qunming Wang, Wenzhong Shi, Peter M. Atkinson and Qi Wei

***Abstract*—Area-to-point regression kriging (ATPRK) is an advanced image fusion approach in remote sensing. In this paper, ATPRK is considered for sharpening hyperspectral images (HSIs), based on the availability of a fine spatial resolution panchromatic or multispectral image. ATPRK can be used straightforwardly to sharpen each coarse hyperspectral band in turn. This scheme, however, is computationally expensive due to the large number of bands in HSIs, and this problem is exacerbated for multi-scene or multi-temporal analysis. Thus, we extend ATPRK for fast HSI sharpening with a new approach, called approximate ATPRK (AATPRK), which transforms the original HSI to a new feature space and image fusion is performed for only the first few components before back-transformation. Experiments on two HSIs show that AATPRK greatly expedites ATPRK, but inherits the advantages of ATPRK, including maintaining a very similar performance in sharpening (both ATPRK and AATPRK can produce more accurate results than seven benchmark methods) and precisely conserving the spectral properties of coarse HSIs.**

***Index Terms*—Downscaling, sharpening, image fusion, geostatistics, area-to-point regression kriging (ATPRK), hyperspectral image.**

I. INTRODUCTION

The abundant spectral information available from hyperspectral images (HSIs) provides new opportunities to analyze materials covering the Earth's surface. The high dimensionality of HSI (usually composed of over 100 bands) poses new processing challenges and it has motivated considerable research over the past decades [1]-[5]. Due to the limited amount of incident energy, a tradeoff results between the spatial resolution and spectral resolution. In remote sensing, a fine spatial resolution is frequently needed for reliable image interpretation, for example, for target detection and classification. It is, thus, of great interest to increase the spatial resolution of HSIs with computer technologies, such as image fusion, that combine HSIs with coarse spectral resolution, but fine spatial resolution multispectral images (MSI) or panchromatic (PAN) images [6]. For clarity, in this paper, we term correspondingly these two cases in HSI sharpening as MS-sharpening and pan-sharpening.

Image fusion techniques such as pan-sharpening were originally designed for MSI sharpening [7], [8], for example, fusing MSIs (e.g., four-band 2.4 m QuickBird image) with a PAN image (e.g., single band 0.6 m QuickBird PAN image) acquired over the same scene to produce sharpened MSIs (e.g., four-band 0.6 m QuickBird image). In recent years, with the increasing availability of HSIs and their increasing popularity, HSI sharpening has been identified as an active topic in remote sensing [6]. MSI sharpening methods, such as principal component analysis (PCA) [9]-[11], smoothing filter-based intensity modulation (SFIM) [12], Gram-Schmidt (GS) transformation [13], and adaptive GS (GSA) [14], can be applied straightforwardly to HSI sharpening [15]. However, the two types of issues should be noted.

HSI sharpening is physically different from MSI sharpening. For MSI sharpening, the fine spatial resolution PAN and coarse spatial resolution MSI images are almost in the same spectral range, that is, the visible spectral range (0.4–0.8 μm). For HSI sharpening, however, the spectral range of HSIs commonly covers additionally the shortwave infrared range (0.8–2.5 μm) that is not covered by the fine spatial resolution PAN or MSI. On the other hand, MSI sharpening usually involves pan-sharpening, while HSI sharpening can sometimes involve MS-sharpening, which is a case of hyper-sharpening, a terminology presented in a recent publication [16]. MS-sharpening can be viewed as an extension of pan-sharpening, where the fine spatial resolution source in pan-sharpening (i.e., single band PAN) is extended to a set of bands. Correspondingly, appropriate mathematical models need to be identified for MS-sharpening.

HSI sharpening has received increasing attention and several approaches have been developed. Apart from the methods originally designed for MSI sharpening (e.g., SFIM, PCA, GS and GSA), some other methods exist, including guided filter PCA (GFPCA) [17], coupled nonnegative matrix factorization (CNMF) [18], sparse representation [19]-[20], Bayesian approaches (including Bayesian Naïve [21], Bayesian Sparse [22] and HySure [23]) [21]-[24], and hybrid approaches [25]. The methods in [17]-[25] can be used for both pan-sharpening and MS-sharpening. It is beyond the scope of this paper to explicitly introduce the existing hyperspectral sharpening approaches, but a recent review on them exists [6].

In this paper, we propose an area-to-point regression kriging (ATPRK)-based geostatistical solution for HSI sharpening. ATPRK was originally proposed for downscaling 500 m MODIS bands 3-7 to a spatial resolution of 250 m in our

Manuscript received November 11, 2015; revised March 4, 2016 and April 14, 2016; accepted May 3, 2016. This work was supported in part by the Research Grants Council of Hong Kong under Grant PolyU 15223015 and 5249/12E, in part by the National Natural Science Foundation of China under Grant 41331175, in part by the Leading talent Project of National Administration of Surveying under grant K.SZ.XX.VTQA, and in part by the Ministry of Science and Technology of China under Grant 2012BAJ15B04 and Project 2012AA12A305.
(Corresponding author: W. Shi.)

Q. Wang is with the Lancaster Environment Centre, Lancaster University, Lancaster LA1 4YQ, UK and the Department of Land Surveying and Geo-Informatics, The Hong Kong Polytechnic University, Hong Kong (e-mail: wqm11111@126.com).

W. Shi is with The Hong Kong Polytechnic University, Hong Kong, and also with Wuhan University, Wuhan 430072, China (e-mail: lswzshi@polyu.edu.hk).

P.M. Atkinson is with the Faculty of Science and Technology, Lancaster University, Lancaster LA1 4YR, UK; School of Geography, Archaeology and Palaeoecology, Queen's University Belfast, BT7 1NN, Northern Ireland, UK; and also with Geography and Environment, University of Southampton, Highfield, Southampton SO17 1BJ, UK (e-mail: pma@lancaster.ac.uk).

Q. Wei is with Department of Engineering, University of Cambridge, Cambridge CB2 1PZ, UK (qw245@cam.ac.uk).

previous work [26]. The terminology "downscaling" in this paper means increasing the spatial resolution of images and coveys the same meaning of sharpening. ATPRK explicitly accounts for the size of support, spatial correlation, and the point spread function (PSF) of the sensor and has the significant advantage of precisely preserving the spectral properties of the observed coarse data and the ease of incorporating multiple covariates (i.e., fine spatial resolution sources in image fusion). As illustrated in our previous works [26], [27], ATPRK is more user-friendly than other geostatistical solutions for sharpening such as kriging with external drift [28] and downscaling cokriging [29]. Moreover, the advanced approach was demonstrated to outperform 13 current state-of-the-art benchmarks in pan-sharpening MSIs in our previous work [30]. Motivated by the advantages and encouraging performances in sharpening MSIs (e.g., MODIS and Landsat images), ATPRK is further considered for sharpening HSI in this paper.

Naturally, when applied to HSI sharpening, ATPRK can be used to sharpen each coarse band in turn, as was done in downscaling MODIS images. This scheme for HSI sharpening, however, is computationally expensive due to the large number of bands in HSIs. Moreover, often users need to downscale more than one scene, for example, multiple scenes for subsequent mosaicing. Last but not least, when applied to continuous monitoring, ATPRK needs to be repeated multiple times to analyze time-series images (e.g., 100 times for 100 dates in a time-series).

In view of the computational cost, in this paper, an extended version of the advanced ATPRK approach, termed approximate ATPRK (AATPRK), is proposed for fast HSI sharpening. In HSI, there exists great correlation between bands and redundant information in original large number of bands. The proposed AATPRK approach transforms the original HSI data to a new feature space where only the few components containing most of the information are sharpened, thereby greatly save the computing time. The main contributions of AATPRK lie in noticeably expediting the advanced ATPRK approach in HSI sharpening but maintaining the sharpening accuracy. The expedited version will extend the use of ATPRK in multi-scene and multi-temporal analysis based on HSI.

AATPRK holds the following characteristics and advantages.

1) AATPRK can greatly expedite the ATPRK-based processing required for HSI sharpening and meanwhile maintain the performance in sharpening.
2) Inheriting the appealing advantage of ATPRK (i.e., the perfect coherence), AATPRK can almost perfectly preserve the spectral properties of the original coarse HSI.
3) Inheriting the advantages of ATPRK, AATPRK can be straightforwardly extended from pan-sharpening to MS-sharpening, thus facilitating the application in various data fusion (such as fusion of Hyperion and ASTER [31]). For MS-sharpening, each band of the fine spatial resolution MSI is considered as a covariate (i.e., auxiliary data) and multiple regression between the primary variable (i.e., observed coarse HSI bands) and covariates is involved.

The remainder of this paper is organized into four sections. Section II introduces the principles of the AATPRK-based HSI sharpening approach. The experimental results for two HSI datasets are provided in Section III to demonstrate the applicability of AATPRK. Section IV further discusses the proposed approach, followed by a conclusion in Section V.

II. Methods

Let $Z_V^l(\mathbf{x}_i)$ be the measurements of coarse spatial resolution pixel V centered at $\mathbf{x}_i$ ($\mathbf{x}$ is a two-dimension coordinate vector denoting the spatial locations of pixels; i=1,…,M, where M is the number of pixels) in coarse band l (l=1,…,L, where L is the number of HSI bands), and $Z_v^k(\mathbf{x}_j)$ be the measurements of fine spatial resolution pixel v centered at $\mathbf{x}_j$ (j=1,…, MF^2, where F is the spatial resolution (zoom) ratio between the coarse and fine spatial resolution bands) in fine spatial resolution band (hereafter fine band) k (k=1,…,K, where K is the number of fine MSI bands) in the fine MSI. The objective of HSI sharpening is to predict $Z_v^l(\mathbf{x})$ for all fine pixels in all L coarse bands.

Since pan-sharpening can be viewed as a particular case of MS-sharpening and the mathematical models for both cases become the same when K=1, we only present the more general MS-sharpening case (i.e., fusion of $Z_V^l(\mathbf{x}_i)$ and $Z_v^k(\mathbf{x}_j)$) in this section.

A. *Transforming the coarse HSI to a new feature space*

In HSI, the number of bands is large and the correlation between bands (particularly for spectrally neighboring ones) is very large. To reduce the computational burden in ATPRK-based HSI sharpening, some transformation of the original HSI is considered. The proposed fast AATPRK approach starts from projection of the HSI into a new feature space in which the components are uncorrelated, with the overall brightness variance in the original HSI condensed to a few components and the spectral shape retained by the remaining components. In the new feature space, only the components that contain most of the variance need to be sharpened using the fine MSI, which reduces the computational cost.

In this paper, the well-known PCA is used for the feature space transformation. PCA works by linearly transforming the original data, and the variance in the original HSI is rearranged and the first few principal components (PCs) contain almost all of the variance in the original data [32]. In AATPRK, the first L_0 ($L_0 << L$) PCs are sharpened using the fine MSI. In this paper, the first L_0 PCs that contain over 99% of the information (quantified in terms of cumulative eigenvalues) are considered. The fusion scheme of sharpening only few components in a low-dimensional subspace was adopted in several studies. For example, Liao *et al*. [17] sharpened the first few PCs in the PC subspace using a guided filter. Simoes *et al*. [23] formulated the HSI sharpening problem as the minimization of a convex objective function and solved the problem in the low-dimensional subspace by the split augmented Lagrangian shrinkage algorithm.

B. *Sharpening PCs with ATPRK*

In the new space found by PCA, almost all variance in the original HSI is condensed to the first L_0 PCs. ATPRK is used to sharpen the L_0 PCs where each PC is considered as a primary variable and the available MSI provides the covariate set. That is, the coarse PC images are fused with the fine spatial resolution MSI. Suppose $Y_V^l(\mathbf{x}_i)$ is the measurements of pixel *V* centered at $\mathbf{x}_i$ in coarse band *l* (*l*=1,…,*L*) in the new feature space after PCA-based transformation. The first L_0 bands in the new space are sharpened by ATPRK, treating the fine MSI as a set of covariates. ATPRK is a two-step approach consisting of regression modelling and area-to-point kriging (ATPK)-based residual downscaling.

The prediction of the first step (i.e., regression modelling) in ATPRK is a linear combination of all fine spatial resolution bands in MSI (see (4)). Normally, there exists bias between the regression prediction and the observed coarse data. In the second step, the coarse spatial resolution residuals from the regression model in the first step (see (3)) are downscaled to the fine spatial resolution using ATPK (see (5)), where the coarse residuals can be retained perfectly. The fine spatial resolution residuals are added to back to the regression prediction in the first step to produce the final sharpened result (see (1)). In ATPK-based residual downscaling, the size of support, spatial correlation (characterized by the relation between residuals), and the PSF of the HSI sensor (see (7) and (8)) are explicitly accounted for. The final ATPRK prediction has perfect coherence with the observed coarse HSI, that is, when the ATPRK result is degraded to the coarse spatial resolution, it is exactly the same as the observed coarse HSI.

Let $\hat{Y}_{v1}^l(\mathbf{x})$ and $\hat{Y}_{v2}^l(\mathbf{x})$ be the predictions of regression and ATPK, respectively, for band *l*. The ATPRK prediction is calculated as

$$\hat{Y}_v^l(\mathbf{x}) = \hat{Y}_{v1}^l(\mathbf{x}) + \hat{Y}_{v2}^l(\mathbf{x}) . \tag{1}$$

The regression prediction is calculated by taking full advantage of the fine spatial resolution textural information in the *K* covariates (i.e., fine bands) of the MSI. First, the MSI is upscaled band-to-band to match the spatial resolution of the coarse PCs. Denoting the *k*th upscaled band of MSI as Z_V^k, it is calculated as

$$Z_V^k = h_V^k(\mathbf{x}) * Z_v^k(\mathbf{x}) \tag{2}$$

where * is the convolution operator and $h_V^k(\mathbf{x})$ is the PSF for the *k*th band of the MSI sensor. The relationship between the two types of coarse images is modelled by multiple linear regression and the regression model for band *l* is described as

$$Y_V^l(\mathbf{x}) = \sum_{k=0}^{K} a_k^l Z_V^k(\mathbf{x}) + R_l(\mathbf{x}),\ Z_V^0(\mathbf{x}) = 1\ \forall \mathbf{x} \tag{3}$$

where $R_l(\mathbf{x})$ is a residual term and a_0^l is the intercept. The coefficients $\{a_k^l \mid k = 1,...,K\}$ can be estimated by ordinary least squares. Based on the assumption of scale-invariance, the regression model in (3) is used for regression prediction at the fine spatial resolution. For a specific location $\mathbf{x}_0$, (4) holds

$$\hat{Y}_{v1}^l(\mathbf{x}_0) = \sum_{k=0}^{K} a_k^l Z_v^k(\mathbf{x}_0),\ Z_v^0(\mathbf{x}_0) = 1 . \tag{4}$$

To retain the spectral information in the original coarse data, ATPK-based residual downscaling is performed as a complement to the regression step. ATPK downscales the coarse residual image $R_l(\mathbf{x})$ to the fine spatial resolution. Specifically, the fine residual at a specific location $\mathbf{x}_0$ is a linear combination of its neighboring coarse residuals

$$\hat{Y}_{v2}^l(\mathbf{x}_0) = \sum_{i=1}^{N} \lambda_i R_l(\mathbf{x}_i),\ \text{s.t.}\ \sum_{i=1}^{N} \lambda_i = 1 \tag{5}$$

where λ_i is the weight for the *i*th coarse residual centered at $\mathbf{x}_i$ and *N* is the number of neighboring coarse pixels, such as the *N*=5×5 window of coarse pixels in this paper (a larger window size will not necessarily lead to a greater accuracy, but will certainly lead to longer computing time). The weights $\{\lambda_i \mid i = 1,..., N\}$ are calculated according to the kriging matrix below

$$\begin{bmatrix} \gamma_{VV}^l(\mathbf{x}_1,\mathbf{x}_1) & \dots & \gamma_{VV}^l(\mathbf{x}_1,\mathbf{x}_N) & 1 \\ . & . & . & . \\ . & . & . & . \\ . & . & . & . \\ \gamma_{VV}^l(\mathbf{x}_N,\mathbf{x}_1) & \dots & \gamma_{VV}^l(\mathbf{x}_N,\mathbf{x}_N) & 1 \\ 1 & \dots & 1 & 0 \end{bmatrix} \begin{bmatrix} \lambda_1 \\ . \\ . \\ . \\ \lambda_N \\ \theta \end{bmatrix} = \begin{bmatrix} \gamma_{vV}^l(\mathbf{x}_0,\mathbf{x}_1) \\ . \\ . \\ . \\ \gamma_{vV}^l(\mathbf{x}_0,\mathbf{x}_N) \\ 1 \end{bmatrix} \tag{6}$$

in which $\gamma_{VV}^l(\mathbf{x}_i,\mathbf{x}_j)$ is the coarse-to-coarse semivariogram between coarse pixels centered at $\mathbf{x}_i$ and $\mathbf{x}_j$ in band *l*, $\gamma_{vV}^l(\mathbf{x}_0,\mathbf{x}_j)$ is the fine-to-coarse semivariogram between fine and coarse pixels centered at $\mathbf{X}_0$ and $\mathbf{x}_j$ in band *l*, and θ is the Lagrange multiplier of the term accounting for the sum-to-one constraint on the weights in (5).

Suppose **s** is the Euclidean distance between the centroids of any two pixels and $h_V^l(\mathbf{s})$ is the PSF for the *l*th band of the HSI sensor. $\gamma_{VV}^l(\mathbf{s})$ and $\gamma_{vV}^l(\mathbf{s})$ in (6) are calculated by convoluting the fine-to-fine semivariogram $\gamma_{vv}^l(\mathbf{s})$ with the PSF $h_V^l(\mathbf{s})$ as follows

$$\gamma_{vV}^l(\mathbf{s}) = \gamma_{vv}^l(\mathbf{s}) * h_V^l(\mathbf{s}) \tag{7}$$

$$\gamma_{VV}^l(\mathbf{s}) = \gamma_{vv}^l(\mathbf{s}) * h_V^l(\mathbf{s}) * h_V^l(-\mathbf{s}) \tag{8}$$

where $\gamma_{vv}^l(\mathbf{s})$ can be estimated by deconvolution of the coarse semivariogram calculated from the coarse residual image $R_l(\mathbf{x})$. Readers may refer to [26], [27], [30] for details on the deconvolution approach. The sensor PSF can be the one in (9), based on the hypothesis that the coarse pixel value is the average of the fine pixel values within it [33]

$$h_V(\mathbf{x}) = \begin{cases} \dfrac{1}{S_V}, & \text{if } \mathbf{x} \in V(\mathbf{x}) \\ 0, & \text{otherwise} \end{cases} \tag{9}$$

in which S_V is the size of pixel *V* and $V(\mathbf{x})$ is the spatial support (i.e., spatial coverage) of pixel *V* centered at **x**.

C. AATPRK

In AATPRK, the first L_0 PCs are fused with the fine spatial resolution MSI using ATPRK. For the remaining *L*-L_0 low-ranking PCs, they are assumed to contain little variance (i.e., textural information) and only used to preserve the spectral shape of the observed HSI data. Thus, the low-ranking PCs are downscaled to the fine spatial resolution with the simple and fast bicubic interpolation instead. The downscaled HSI in the new feature space is finally transformed back to the original feature space by inverse PCA. The implementation of the proposed AATPRK is summarized as follows.

1) The original coarse HSI $\{Z_V^l(\mathbf{x}_i) \mid i=1,...,M; l=1,...,L\}$ is transformed to the new feature space $\{Y_V^l(\mathbf{x}_i) \mid i=1,...,M; l=1,...,L\}$ by PCA.
2) The first L_0 PCs are downscaled to $\{\hat{Y}_v^l(\mathbf{x}_i) \mid i=1,...,MF^2; l=1,...,L_0\}$ using ATPRK, where the available MSI $\{Z_v^k(\mathbf{x}_j) \mid j=1,...,MF^2; k=1,...,K\}$ is treated as the covariate set, as illustrated in Section II-B.
3) The remaining L-L_0 PCs are downscaled to $\{\hat{Y}_v^l(\mathbf{x}_i) \mid i=1,...,MF^2; l=L_0+1,...,L\}$ with fast bicubic interpolation.
4) Inverse transformation is performed to transform the downscaled L PCs $\{\hat{Y}_v^l(\mathbf{x}_i) \mid i=1,...,MF^2; l=1,...,L\}$ back to the original feature space $\{\hat{Z}_v^l(\mathbf{x}_i) \mid i=1,...,MF^2; l=1,...,L\}$.

Fig. 1 is a flowchart describing the proposed AATPRK approach. The semivariogram modelling process (including deconvolution and convolution) in ATPRK generally takes some time for each band. If the number of bands is small, as for a four-band 2.4 m Quickbird or five-band 500 m MODIS image, the computational efficiency of the original ATPRK-based sharpening approach is acceptable [26]. If the number of bands is large, such as over 100 for a HSI, the cumulative computational cost of ATPRK-based sharpening will become large. The computational cost will further be enlarged for the cases involving multiple scenes or multi-temporal analysis.

The proposed approximate version, AATPRK, greatly reduces the computational cost for HSI sharpening by applying PCA to transform the original HSI to a new feature space where spatial information is concentrated in the first L0 PCs. Sharpening only the first L0 PCs, the computational cost of AATPRK is approximately L_0/L times that of ATPRK (the processes of space transformation and bicubic interpolation are very fast and their computational cost is ignored). For example, for a 200-band (L=200) HSI, usually the first five (L_0=5) PCs are able to contain over 99% of the information. In this case, AATPRK increases the computational efficiency by about 40 times.

AATPRK can be viewed as a special case of ATPRK: when L_0 equals L, all PCs in the new feature space will be sharpened by ATPRK in fact; after inverse PCA, AATPRK will achieve the same performance as ATPRK which sharpens all bands in the original feature space (the original space is a linear transformation of the new one and the two spaces are generally reversible). Thus, AATPRK in this case becomes ATPRK.

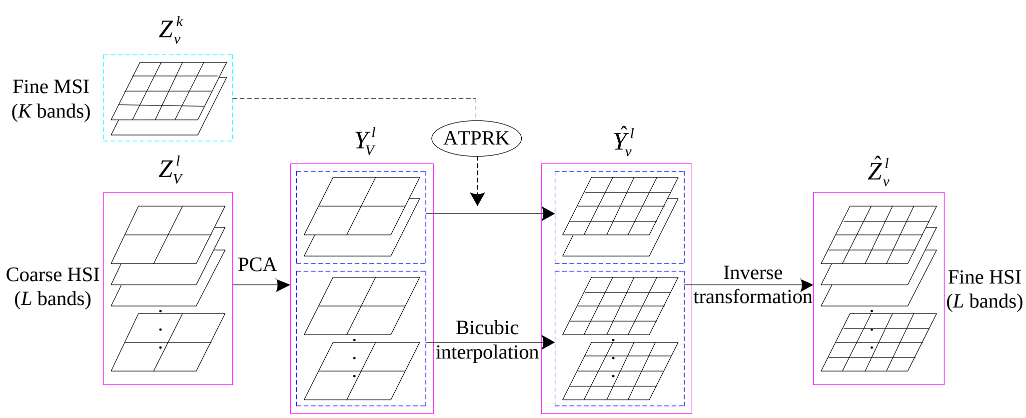

Fig. 1 Flowchart of the proposed AATPRK-based approach for HSI sharpening.

III. Experiments

A. Datasets and experimental setup

The proposed AATPRK approach was examined by two HSIs: the well-known Washington DC and Moffett Field datasets. The spatial extends of the Washington DC and Moffett Field images are 1200 by 300 and 300 by 300 pixels, respectively. After discarding the noisy and water absorption bands, 191 bands of the Washington DC image and 100 bands of the Moffett Field image were retained for the experiments. The spatial resolutions of the two images are 3 m and 20 m, respectively.

In the first experiment, we tested the pan-sharpening case. For both HSIs, all bands were upscaled by a factor of four, simulating 12 m coarse Washington DC and 80 m coarse Moffett Field HSIs. In reality, the PAN image always covers the visible spectral range. To synthesize the fine spatial resolution PAN image, the first 50 bands that fall into the visible spectral range were averaged. The objective of HSI sharpening is to restore the 3 m and 20 m Washington DC and Moffett Field HSIs. For example, for the Washington DC dataset, 3 m HSI was predicted by taking the 12 m HSI as the observed coarse data and 3 m fine PAN as the covariate. Using synthetic data, the reference at the fine spatial resolution is known perfectly, which is critical for reliable assessment. Moreover, we can concentrate solely on the performance of the sharpening methods which may be affected by uncertainties in reality (e.g., registration errors).

In the second experiment, MS-sharpening was applied using the Moffett Field dataset. A four-band 20 m Moffett Field MSI was synthesized by averaging 12 consecutive bands of the first 48 bands. The objective of HSI sharpening is to restore the 20 m Moffett Field HSIs, taking the 80 m HSI as the observed coarse data and 20 m fine MSI as a covariate set.

We compared AATPRK with seven benchmark methods: SFIM [12], GS [13], GSA [14], PCA [9], GFPCA [17], CNMF [18] and Bayesian (using Gaussian prior) [21], [34] to show the accuracy gains of AATPRK in HSI sharpening. AATPRK was also compared with the original ATPRK approach that sharpens all bands in the coarse HSI in turn, to illustrate the capability of AATPRK in maintaining the performance of ATPRK in sharpening. The implementations of SFIM, PCA, GS and GSA in HSI sharpening are the same as those in MSI sharpening. In the GFPCA approach, the first PCs are sharpened with a guided filter [17]. The number of PCs was the same as that in AATPRK, the regularization parameter for the guided filter was set to 10^{-6}, and the local window size was set to 17×17. In CNMF, hyperspectral and multispectral data are alternately unmixed into endmember and abundance matrices, and the final hyperspectral endmember and multispectral abundance matrices are combined to achieve sharpening. The number of endmembers in CNMF was set to 20.

The HSI sharpening results were compared both visually and quantitatively. Five indices were used for quantitative evaluation, including the root mean square error (RMSE), correlation coefficient (CC), relative global-dimensional synthesis error (ERGAS) [35], universal image quality index (UIQI) [36] and spectral angle mapper (SAM). For RMSE, CC and UIQI, they were first calculated for each band, and then the values for all bands were averaged. For SAM, values for spectra of all pixels were first calculated and then averaged.

As mentioned in [37], any sharpened image, once degraded to its original spatial resolution, should be as close as possible to the original image. With this in mind, we also used another index termed coherence (quantified by the CC) for quantitative evaluation. The coherence is measured by the relation between the observed coarse image and the coarse image obtained by upscaling the sharpened image. For each hyperspectral band, a coherence value was calculated and the values for all bands were averaged.

B. Experiment on pan-sharpening

For the Washington DC dataset, the first three PCs contain 87.16%, 10.95% and 1.59% of the information (quantified by dividing the eigenvalue of each PC by the sum of all 191 eigenvalues), respectively, and their cumulative eigenvalues are 99.86%. Thus, the first three PCs were sharpened by ATPRK in AATRPK. With respect to the Moffett Field dataset, the first four PCs were considered (with information proportions of 88.85%, 7.11%, 2.68% and 0.73%, respectively). The pan-sharpening results for the two hyperspectral datasets are shown in Figs. 2-4. Tables 1 and 2 and Figs. 5 and 6 show the quantitative results for the tested methods. Four important observations can be made from the visual and quantitative results.

First, AATPRK is superior to the seven benchmark methods. Visually, the GS, PCA and GFPCA methods lead to obvious spectral distortion. Although SFIM and GSA produce less spectral distortion, the spatial structure is not sufficiently reproduced and the results look ambiguous, especially for the land cover boundaries. Compared with GS, PCA, GFPCA, SFIM and GSA, the CNMF and Bayesian approaches have more satisfactory performances in preserving both the spectral and spatial information, but has a weaker performance in reproducing the spatial details than AATPRK. This can be illustrated by the examples of roof restoration in Fig. 3(g1), Fig. 3(h1) and Fig. 3(i1). The boundaries in Fig. 3(i1) are sharper and clearer than those in Fig. 3(g1) and Fig. 3(h1), and Fig. 3(i1) are closer to the reference in Fig. 3(a1). Checking the values in Tables 1 and 2, AATPRK has a smaller RMSE, ERGAS and SAM, and larger CC, UIQI and coherence values than the seven benchmark methods. Figs. 5 and 6 further reveal that AATPRK produces larger CC than the seven methods for all hyperspectral bands.

Second, all sharpening methods, including AATPRK, tend to have better performances for the bands that have greater correlation (in terms of CC) with the PAN image. As shown in Figs. 5 and 6, the trends of all curves in Fig. 5(a) and Fig. 6(a) are the same as those in Fig. 5(b) and Fig. 6(b). Taking the Washington DC image as an example, in Fig. 5(b), for the first 50 bands, the correlation between them and the PAN image are greater than for the other 141 bands. Correspondingly, for each method, the sharpening accuracy in Fig. 5(a) is the greatest for the first 50 bands. Physically, the reason for this phenomenon is that the first 50 bands fall into the visible spectral range, which is covered by the PAN image. For the remaining 141 bands in the shortwave infrared range, the PAN image provides less relevant fine spatial resolution information for sharpening. Interestingly, in Fig. 5(b), the CC curve reaches a valley point at band 100 and goes up when the band number is larger than 100. As we know, the studied Washington DC area is dominated by vegetation, and the reflectance curve of vegetation reaches a valley point at wavelength 1.4μm, which corresponds to band 100 of the Washington DC hyperspectral data. For bands after the 100th band, the reflectance of vegetation increases and the correlation between their reflectance and those of first 50 bands (or the PAN image) increase as a result. This is not the case in Fig. 6(b), as the studied Moffett Field area is dominated by water. The reflectance of water is large for bands falling into the visible spectral range (bands 1-50) but very small for bands falling into the shortwave infrared range (bands after the 50th band).

Third, the approximation involved in AATPRK greatly expedites ATPRK, but maintaining a very similar performance in sharpening. More precisely, ATPRK took 5921s and 2179s for the Washington DC and Moffett Field HSIs, while AATPRK took only 92s and 86s correspondingly. For the two HSIs, AATPRK increases the computational efficiency by 64 and 25 times, which are generally similar to those calculated from L/L_0 (200/3=67 and 100/4=25). Regarding the accuracy in sharpening, the visual results of the two approaches in Figs. 2-4 are generally the same. Checking the quantitative results in Tables 1 and 2, the accuracy of AATPRK is slightly smaller than that of ATPRK. The accuracy decrease for AATPRK is the cost of reducing the computing time. However, we can see that the differences in quantitative results are also very minor. For example, for the Moffett Field dataset, the CC, UIQI and SAM values of the two methods are even the same. Moreover, the curves in Figs. 5 and 6 for the two methods almost coincide, suggesting that they have almost the same CC for all hyperspectral bands.

Fourth, AATPRK can almost perfectly preserve the spectral properties of the original coarse HSIs. For the two images, AATPRK produces coherence values of 0.9996 and 0.9999, which are very close to the ideal value of 1. This indicates that AATPRK inherits the appealing advantage of perfect coherence of ATPRK.

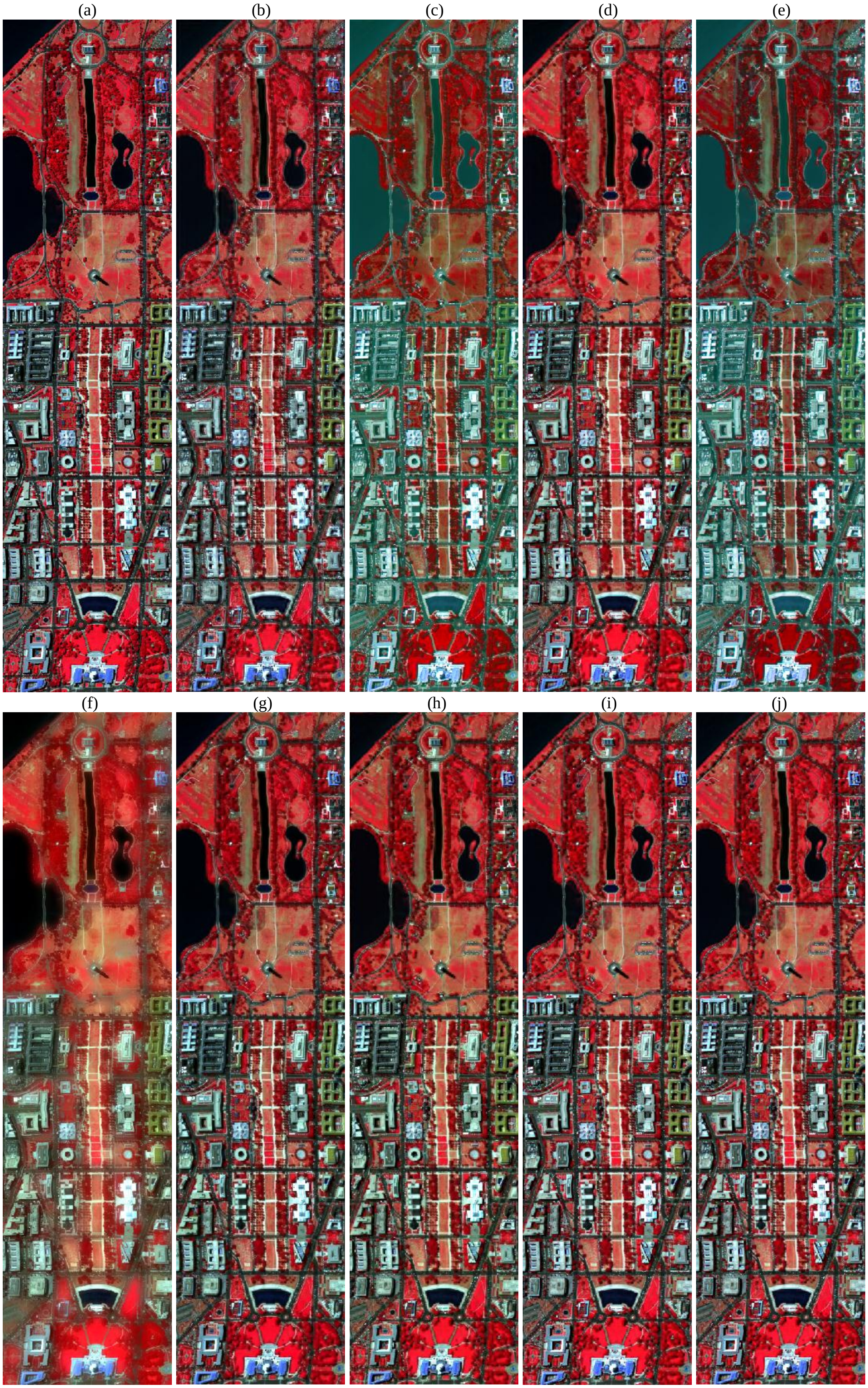

Fig. 2. Pan-sharpening results for the Washington DC dataset (bands 65, 52 and 36 as RGB). (a) 3 m reference image. (b) SFIM. (c) GS. (d) GSA. (e) PCA. (f) GFPCA. (g) CNMF. (h) Bayesian. (i) AATPRK. (j) ATPRK.

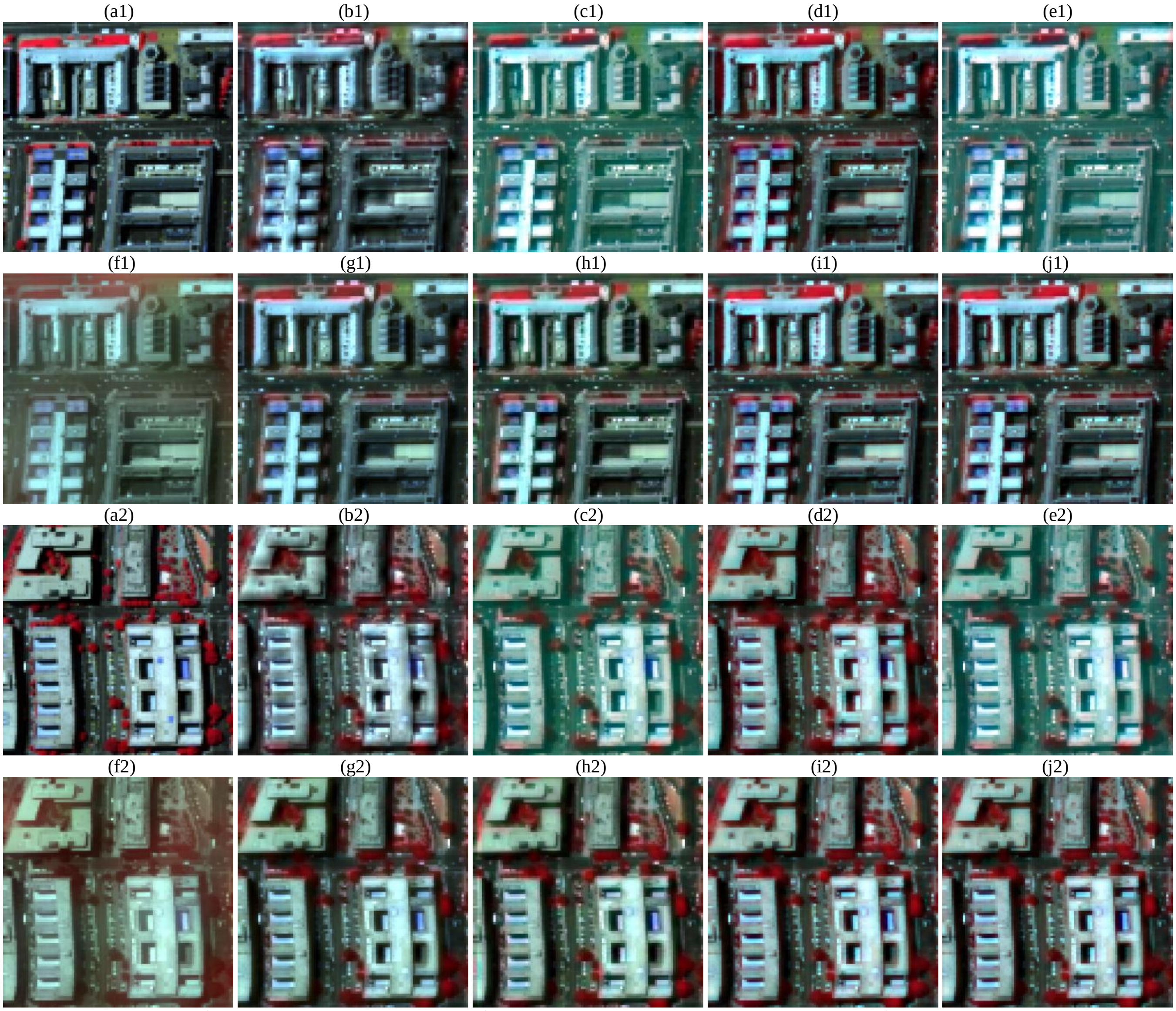

Fig. 3. Pan-sharpening results for two sub-areas in Fig. 2. (a) 3 m reference image. (b) SFIM. (c) GS. (d) GSA. (e) PCA. (f) GFPCA. (g) CNMF. (h) Bayesian. (i) AATPRK. (j) ATPRK.

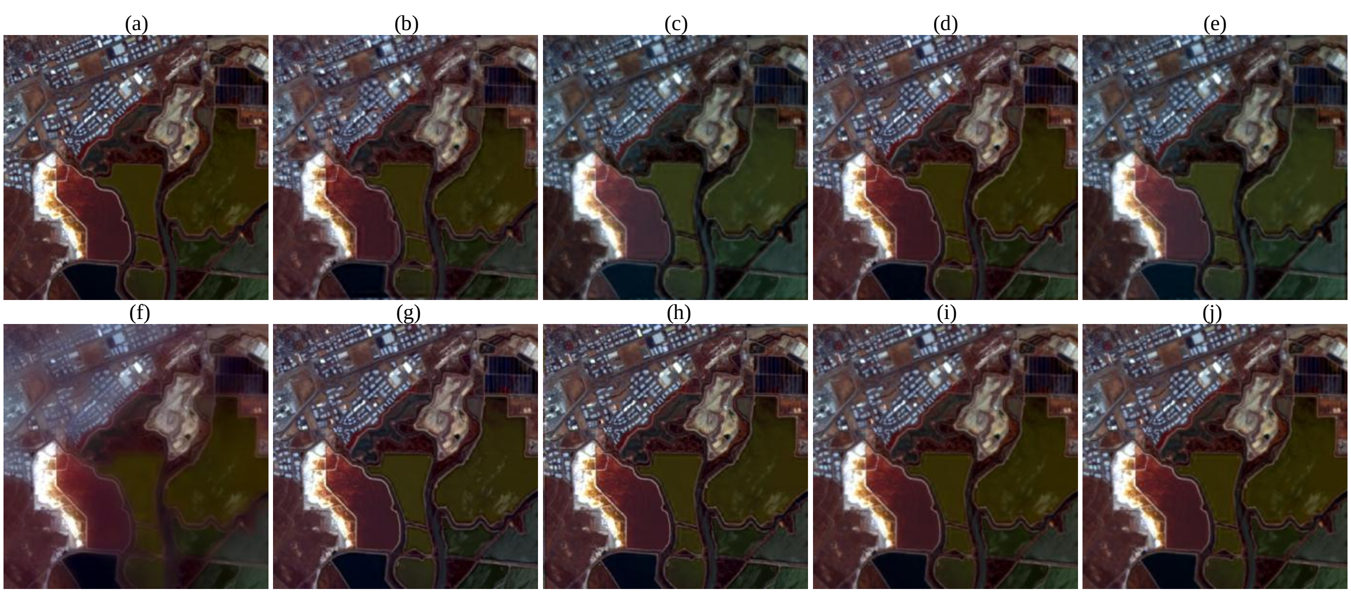

Fig. 4. Pan-sharpening results for the Moffett Field dataset (bands 33, 15 and 4 as RGB). (a) 20 m reference image. (b) SFIM. (c) GS. (d) GSA. (e) PCA. (f) GFPCA. (g) CNMF. (h) Bayesian. (i) AATPRK. (j) ATPRK.

Table 1 Quantitative assessment of the nine pan-sharpening methods for the Washington DC dataset.

	RMSE	CC	ERGAS	UIQI	SAM	Coherence	Time
Ideal	0	1	0	1	0	1	
SFIM	479.4037	0.8779	7.6450	0.8766	0.1713	0.9351	6.2s
GS	556.3292	0.8273	9.0007	0.8057	0.2025	0.8643	7.2s
GSA	323.3304	0.9225	6.2204	0.9198	0.1638	0.9680	7.8s
PCA	605.4827	0.7960	9.6884	0.7768	0.2142	0.8310	16.0s
GFPCA	473.8344	0.8899	7.6409	0.8461	0.1893	0.9333	7.7s
CNMF	288.8795	0.9437	5.3558	0.9394	0.1342	0.9887	38.4s
Bayesian	281.7835	0.9495	5.0367	0.9461	0.1306	0.9976	6.6s
AATPRK	239.4907	0.9583	4.6344	0.9568	0.1201	0.9996	91.5s
ATPRK	239.0927	0.9586	4.6108	0.9573	0.1200	1	5921.0s

Table 2 Quantitative assessment of the nine pan-sharpening methods for the Moffett Field dataset.

	RMSE	CC	ERGAS	UIQI	SAM	Coherence	Time
Ideal	0	1	0	1	0	1	
SFIM	359.7166	0.9406	5.1809	0.9403	0.1124	0.9688	0.8s
GS	369.3218	0.9361	5.6186	0.9274	0.1219	0.9588	0.8s
GSA	255.4487	0.9652	4.2519	0.9649	0.1079	0.9854	1.0s
PCA	334.8550	0.9475	5.1285	0.9400	0.1183	0.9700	1.7s
GFPCA	346.2622	0.9480	4.9651	0.9384	0.1131	0.9727	1.3s
CNMF	192.6305	0.9809	3.0786	0.9804	0.0833	0.9983	7.0s
Bayesian	189.5725	0.9814	3.0535	0.9811	0.0818	0.9998	0.8s
AATPRK	178.0132	0.9835	2.9215	0.9834	0.0744	0.9999	85.7s
ATPRK	177.7196	0.9835	2.9185	0.9834	0.0743	1	2179.0s

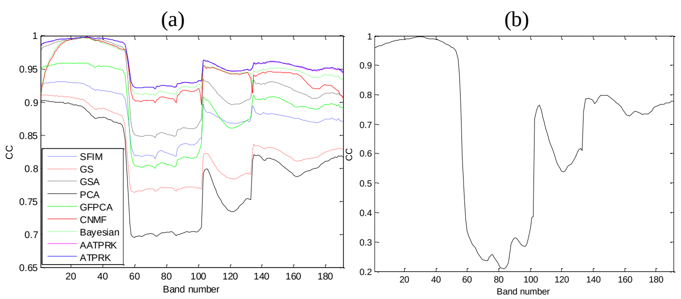

Fig. 5. (a) CC of the nine pan-sharpening methods for each band of the Washington DC dataset (for each CC curve, it contains 191 values for 191 bands and each value means the CC between the sharpened band and the corresponding 3 m reference band). (b) CC between the PAN and each band of the dataset.

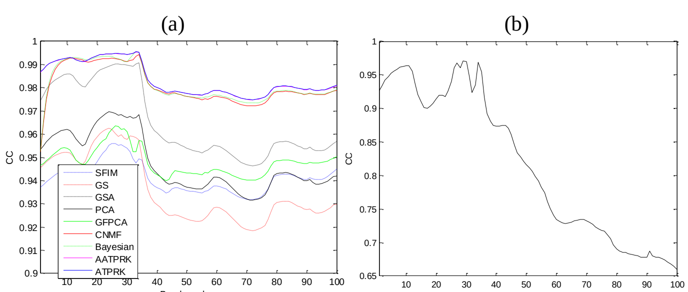

Fig. 6. (a) CC of the nine pan-sharpening methods for each band of the Moffett Field dataset (for each CC curve, it contains 100 values for 100 bands and each value means the CC between the sharpened band and the corresponding 20 m reference band). (b) CC between the PAN and each band of the dataset.

C. Experiment on MS-sharpening

In the second experiment, MS-sharpening for the Moffett Field dataset was conducted. GFPCA, Bayesian and CNMF are methods that can be used to fuse coarse HSIs and fine MSIs. Thus, the three methods were selected as benchmark methods. The visual results are shown in Fig. 7, while the quantitative results are shown in Table 3 and Fig. 8. Similarly, ATPRK and AATPRK produce highly similar results, which are more accurate than GFPCA, Bayesian and CNMF. Moreover, the approximation involved in AATPRK greatly expedites ATPRK (the computing time is decreased from 2165s to 86s) and can also precisely preserve the spectral properties of the original coarse hyperspectral data. The results in this experiment suggest that the proposed AATPRK approach can be used for fusing coarse HSIs and fine MSIs.

Table 3 Quantitative assessment of the five MS-sharpening methods for the Moffett Field dataset.

	RMSE	CC	ERGAS	UIQI	SAM	Coherence	Time
Ideal	0	1	0	1	0	1	
GFPCA	288.6597	0.9658	3.8846	0.9597	0.0702	0.9877	6.3s
CNMF	67.0049	0.9962	1.5385	0.9960	0.0298	0.9993	10.3s
Bayesian	84.5843	0.9952	1.6218	0.9951	0.0342	0.9998	5.0s

AATPRK	60.2501	0.9968	1.4030	0.9968	0.0267	0.9999	86.0s
ATPRK	57.9425	0.9969	1.3867	0.9969	0.0258	1	2164.5s

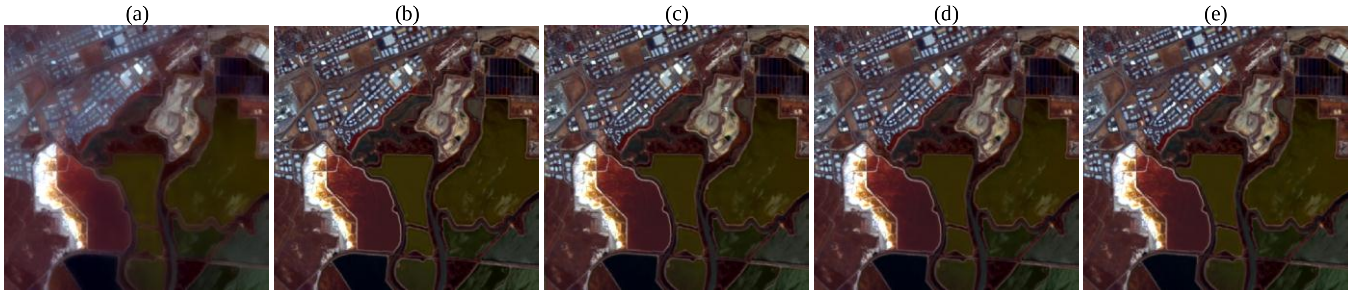

Fig. 7. MS-sharpening results for the Moffett Field dataset (bands 33, 15 and 4 as RGB). (a) GFPCA. (b) CNMF. (c) Bayesian. (d) AATPRK. (e) ATPRK.

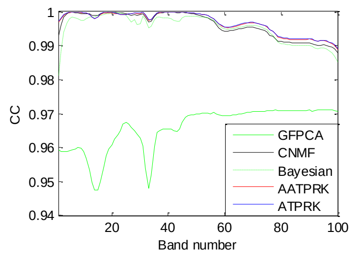

Fig. 8. CC of the five MS-sharpening methods for each band of the Moffett Field dataset (for each CC curve, it contains 100 values for 100 bands and each value means the CC between the sharpened band and the corresponding 20 m reference band).

IV. Discussion

The recently developed ATPRK approach has been shown to be effective in multispectral image sharpening [26], [27], [30]. In this paper, for fast HSI sharpening, the advanced ATPRK approach was extended with an approximate version, AATPRK, which utilizes PCA to transform the original HSI to a new feature space and sharpening is performed for only the first few PCs. The experimental results consistently show that AATPRK produces very nearly the same accuracy as ATPRK, but greatly increases the computational efficiency. This means that the first few PCs are sufficiently to capture the brightness variance of the original HSIs and the PCA-based transformation for HSIs is nearly lossless. Thus, AATPRK is a powerful alternative for ATPRK in HSI sharpening.

ATPRK has the appealing advantages of precisely conserving the spectral properties of the original coarse data and the ease of incorporating multiple covariates. As an extension for HSI sharpening, AATPRK makes full use of the advantages of ATRPK. It fuses coarse HSIs and fine MSIs by treating the fine MSI as a set of covariates (with each band of the MSI being a covariate) and all covariates (i.e., fine bands) are straightforwardly used in image fusion by multiple regression, see (3) and (4). This scheme can take full advantage of the information in the fine MSI, and is substantially different from the alternative solutions identified for hyper-sharpening (i.e., MS-sharpening in this paper) in [16], such as selecting a single band from a fine MSI or synthesizing a single band from a fine MSI (e.g., averaging all fine multispectral bands).

On the other hand, based on the coherence advantage of ATPRK, when sharpening the critical, first few PCs in AATPRK, the information at the coarse spatial resolution is perfectly retained by ATPRK, thereby preserving the variance in the original data. This is the key factor enabling AATPRK to precisely preserve the spectral properties of the observed coarse HSI.

Comparing the results in the two experiments, it can be seen that the accuracy of MS-sharpening is greater than that for pan-sharpening (see Tables 2 and 3). This is because the fine MSI characterizes the fine spatial resolution information more explicitly through multiple bands, rather than the single band in PAN. This finding also encourages the use of more fine bands, including those even in the shortwave infrared range, for possible enhancement of HSI sharpening. Furthermore, some other relevant information (e.g., topographic maps, thematic maps, feild measurements) on the studied areas is also worthy of consideration.

Apart from PCA in this paper, it is also worthwhile to seek alternatives for feature space transformation under the theoretical basis of AATPRK. The transformation is required to condense the information in the original large number of bands into several bands, and it needs to be as lossless as possible to ensure information in the original HSI is retained to the largest extent possible and that the spaces are reversible. For example, it would be interesting to use a small number of reflectance basis functions (i.e., basis image planes) to characterize the entire HSI (such that each hyperspectral band is viewed as a linear combination of the basis functions) [38]. Sharpening only the small number of basis image planes will greatly speed up the process required for HSI sharpening. How to determine the basis functions and the weights would be critical issues. This is part of our ongoing research.

As observed from the studied scene (Fig.2(a) and Fig. 4(a)), the spatial content (i.e., the land-cover/land-use class) may sometimes vary greatly from area to area [39]. For example, in the Moffett Field image, the top left corner region is dominated by the buildings, while the other region is covered by other land cover classes (e.g., water). In AATPRK, a global scheme is considered for sharpening each coarse PC. Spatially adaptive schemes that are able to account for the variation of spatial structure locally provide promising avenues for future research. The idea could be the construction of a local regression model or a local ATPK-based residual downscaling approach, or both.

V. Conclusion

This paper extends the advanced ATPRK approach with an approximate version, AATPRK, for fast HSI sharpening. First, the HSI is transformed to a new feature space by PCA to compress the spatial information in the original HSI into several

PCs. Then, only for the first few PCs, they are sharpened with ATPRK, treating the fine PAN or MSI as the covariate set. For the remaining PCs, they are downscaled to the fine spatial resolution with the simple and fast bicubic interpolation technique. Finally, inverse PCA is performed to produce the fine spatial resolution HSI. The proposed AATPRK approach was assessed using two HSIs, and its performance was compared to that of seven benchmark methods (i.e., SFIM, GS, GSA, PCA, GFPCA, CNMF and Bayesian) in the experiments. The findings are summarized as follows.

1) AATPRK can produce more accurate sharpening results than the seven benchmark methods.
2) The approximation involved in AATPRK greatly expedites ATPRK, but maintaining a very similar performance in sharpening.
3) AATPRK can precisely preserve the spectral properties of the observed coarse HSIs.

ACKNOWLEDGMENT

This work was supported in part by the Research Grants Council of Hong Kong under Grant PolyU 15223015 and 5249/12E, in part by the National Natural Science Foundation of China under Grant 41331175, in part by the Leading talent Project of National Administration of Surveying under grant K.SZ.XX.VTQA, and in part by the Ministry of Science and Technology of China under Grant 2012BAJ15B04 and Project 2012AA12A305. The authors would like to thank the authors in Reference [6] for sharing their code for pan-sharpening algorithms at http://www.openremotesensing.net.

REFERENCES

[1] A. Plaza, et al, “Recent advances in techniques for hyperspectral image processing,” *Remote Sensing of Environment*, vol. 113, pp. S110–S122, 2009.
[2] J. M. Bioucas-Dias, A. Plaza, G. Camps-Valls, P. Scheunders, N. Nasrabadi, and J. Chanussot, “Hyperspectral remote sensing data analysis and future challenges,” *IEEE Geoscience and Remote Sensing Magazine*, vol. 1, no. 2, pp. 6–36, 2013.
[3] J. M. Bioucas-Dias, A. Plaza, N. Dobigeon, M. Parente, Q. Du, P. Gader, and J. Chanussot, “Hyperspectral unmixing overview: Geometrical, statistical and sparse regression-based approaches,” *IEEE Journal of Selected Topics in Applied Earth Observations and Remote Sensing*, vol. 5, no. 2, pp. 354–379, 2012.
[4] M. Fauvel, Y. Tarabalka, J. A. Benediktsson, J. Chanussot, J. C. Tilton, “Advances in spectral–spatial classification of hyperspectral images,” *Proceedings of the IEEE*, vol. 101, no. 3, pp. 652–675, 2012.
[5] L. Wang, S. Hao, Q. Wang, and Y. Wang. Semi-supervised classification for hyperspectral imagery based on spatial-spectral label propagation. *ISPRS Journal of Photogrammetry and Remote Sensing*, vol. 97, pp. 123–137, 2014.
[6] L. Loncan, et al, “Hyperspectral pansharpening: a review,” *IEEE Geoscience and Remote Sensing Magazine*, vol. 3, no. 3, pp. 27–46, 2015.
[7] G. Vivone, L. Alparone, J. Chanussot, M. Dalla Mura, A. Garzelli, G. A. Licciardi, R. Restaino, and L. Wald, “A critical comparison among pansharpening algorithms,” *IEEE Transactions on Geoscience and Remote Sensing*, vol. 53, no. 5, pp. 2565–2586, 2015.
[8] C. Pohl and J. L. Van Genderen, “Review article Multisensor image fusion in remote sensing: Concepts, methods and applications,” *International Journal of Remote Sensing*, vol. 19, no. 5, 823–854, 1998.
[9] V. K. Shettigara, “A generalized component substitution technique for spatial enhancement of multispectral images using a higher resolution data set,” *Photogrammetric Engineering and Remote Sensing*, vol. 58, no. 5, pp. 561–567, 1992.
[10] V. P. Shah, N. H. Younan, and R. L. King, “An Efficient Pan-Sharpening Method via a Combined Adaptive PCA Approach and Contourlets,” *IEEE Transactions on Geoscience and Remote Sensing*, vol. 46, no. 5, pp. 1323–1335, 2008.
[11] K. Rong, L. Jiao, S. Wang, and F. Liu, “Pansharpening Based on Low-Rank and Sparse Decomposition,” *IEEE Journal of Selected Topics in Applied Earth Observations and Remote Sensing*, vol. 7, no. 12, pp. 4793–4805, 2014.
[12] J. G. Liu, “Smoothing filter based intensity modulation: A spectral preserve image fusion technique for improving spatial details,” *International Journal of Remote Sensing*, vol. 21, no. 18, pp. 3461–3472, 2000.
[13] C. A. Laben and B. V. Brower, “Process for enhancing the spatial resolution of multispectral imagery using pan-sharpening,” U.S. Patent 6011875, 2000.
[14] B. Aiazzi, S. Baronti, and M. Selva, “Improving component substitution pansharpening through multivariate regression of MS+Pan data,” *IEEE Transactions on Geoscience and Remote Sensing*, vol. 45, no. 10, pp. 3230–3239, 2007.
[15] G. Vivone, L. Alparone, J. Chanussot, M. Dalla Mura, Garzelli, and G. Licciardi, “Multi-resolution analysis and component substitution techniques for hyperspectral pansharpening,” in *Proceedings of IEEE International Geoscience and Remote Sensing Symposium (IGARSS)*, 2014, pp. 2649–2652.
[16] M. Selva, B. Aiazzi, F. Butera, L. Chiarantini, and S. Baronti, “Hyper-sharpening: A first approach on SIM-GA data,” *IEEE Journal of Selected Topics in Applied Earth Observation and Remote Sensing*, vol. 8, no. 6, pp. 3008–3024, 2015.
[17] W. Liao, et al, “Processing of multiresolution thermal hyperspectral and digital color data: Outcome of the 2014 IEEE GRSS data fusion contest,” *IEEE Journal of Selected Topics in Applied Earth Observation and Remote Sensing*, vol. 8, no. 6, pp. 2984–2996, 2015.
[18] N. Yokoya, T. Yairi, and A. Iwasaki, “Coupled nonnegative matrix factorization unmixing for hyperspectral and multispectral data fusion,” *IEEE Transactions on Geoscience and Remote Sensing*, vol. 50, no. 2, pp. 528–537, 2012.
[19] N. Akhtar, F. Shafait, and A. Mian, “Bayesian sparse representation for hyperspectral image super resolution,” in *Proceedings of IEEE Conference on Computer Vision and Pattern Recognition (CVPR)*, pp. 3631–3640, 2015.
[20] M. A. Veganzones, M. Simoes, G. Licciardi, N. Yokoya, J. M. Bioucas-Dias, and J. Chanussot, “Hyperspectral super-resolution of locally low rank images from complementary multisource data,” *IEEE Transactions on Image Processing*, vol. 25, no. 1, pp. 274–288, 2016.
[21] Q. Wei, N. Dobigeon, and J. Y. Tourneret, “Bayesian Fusion of Multi-Band Images,” *IEEE Journal of Selected Topics in Signal Processing*, vol.9, no.6, pp.1117–1127, 2015.
[22] Q. Wei, J. Bioucas-Dias, N. Dobigeon, and J. Tourneret, “Hyperspectral and multispectral image fusion based on a sparse representation,” *IEEE Transactions on Geoscience and Remote Sensing*, vol. 53, no. 7, pp. 3658–3668, 2015.
[23] M. Simoes, J. Bioucas Dias, L. Almeida, and J. Chanussot, “A convex formulation for hyperspectral image superresolution via subspace-based regularization,” *IEEE Transactions on Geoscience and Remote Sensing*, vol. 53, no. 6, pp. 3373–3388, 2015.
[24] Y. Zhang, S. De Backer, and P. Scheunders, “Noise-resistant wavelet-based Bayesian fusion of multispectral and hyperspectral images,” *IEEE Transactions on Geoscience and Remote Sensing*, vol. 47, no. 11, pp. 3834–3843, 2009.
[25] F. Palsson, J. R. Sveinsson, M. O. Ulfarsson, and J. A. Benediktsson, “Model-based fusion of multi- and hyperspectral images using PCA and wavelets,” *IEEE Transactions on Geoscience and Remote Sensing*, vol. 53, no. 5, pp. 2652–2663, 2015.
[26] Q. Wang, W. Shi, P. M. Atkinson, and Y. Zhao. Downscaling MODIS images with area-to-point regression kriging. *Remote Sensing of Environment*, vol. 166, pp. 191–204, 2015.
[27] Q. Wang, W. Shi, P. M. Atkinson, and E. Pardo-Iguzquiza, “A new geostatistical solution to remote sensing image downscaling,” *IEEE Transactions on Geoscience and Remote Sensing*, vol. 54, no. 1, pp. 386–396, 2016.
[28] M. H. R. Sales, C. M. Souza, Jr., and P. C. Kyriakidis, “Fusion of MODIS images using kriging with external drift,” *IEEE Transactions on Geoscience and Remote Sensing*, vol. 51, no. 4, pp. 2250–2259, 2013.
[29] E. Pardo-Iguzquiza, V. F. Rodrǵuez-Galiano, M. Chica-Olmo, and P. M. Atkinson, “Image fusion by spatially adaptive filtering using downscaling cokriging,” *ISPRS Journal of Photogrammetry and Remote Sensing*, vol. 66, no. 3, pp. 337–346, 2011.

[30] Q. Wang, W. Shi, and P. M. Atkinson, "Area-to-point regression kriging for pan-sharpening," *ISPRS Journal of Photogrammetry and Remote Sensing*, vol. 114, pp. 151–165, 2016.
[31] N. Yokoya, N. Mayumi, and A. Iwasaki, "Cross-Calibration for Data Fusion of EO-1/Hyperion and Terra/ASTER," *IEEE Journal of Selected Topics in Applied Earth Observation and Remote Sensing*, vol. 6, no. 2, pp. 419–426, 2013.
[32] X. Jia and J. A. Richards, "Segmented principal components transformation for efficient hyperspectral remote-sensing image display and classification," *IEEE Transactions on Geoscience and Remote Sensing*, vol. 37, no. 1, pp. 538–542, 1999.
[33] P. M. Atkinson, E. Pardo-Igúzquiza, and M. Chica-Olmo, "Downscaling cokriging for super-resolution mapping of continua in remotely sensed images," *IEEE Transactions on Geoscience and Remote Sensing*, vol. 46, no. 2, pp. 573–580, 2008.
[34] Q. Wei, N. Dobigeon, J. Y. Tourneret, "Fast fusion of multi-band images based on solving a Sylvester equation," *IEEE Transactions on Image Processing*, vol. 24, no. 11, pp. 4109–4121, 2015.
[35] T. Ranchin and L. Wald, "Fusion of high spatial and spectral resolution images: The ARSIS concept and its implementation," *Photogrammetric Engineering and Remote Sensing*, vol. 66, no. 1, pp. 49–61, 2000.
[36] Z. Wang and A. C. Bovik, "A universal image quality index," *IEEE Signal Processing Letters*, vol. 9, no. 3, pp. 81–84, 2002.
[37] L. Wald, T. Ranchin, and M. Mangolini, "Fusion of satellite images of different spatial resolutions: assessing the quality of resulting images," *Photogrammetric Engineering and Remote Sensing*, vol. 63, no. 6, pp. 691–699, 1997.
[38] T. Akgun, Y. Altunbasak, and R. M. Mersereau, "Super-resolution reconstruction of hyperspectral images," *IEEE Transactions on Image Processing*, vol. 14, no. 11, pp. 1860–1875, 2005.
[39] Q. Wang, W. Shi, and H. Zhang, "Class allocation for soft-then-hard subpixel mapping algorithms with adaptive visiting order of classes," *IEEE Geoscience and Remote Sensing Letters*, vol. 11, no. 9, pp. 1494–1498, 2014.

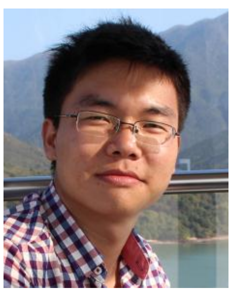

Qunming Wang (M'15) received the B.S. degree and M.S. degree from Harbin Engineering University, Harbin, China, in 2010 and 2012, and the Ph.D. degree from The Hong Kong Polytechnic University, Hong Kong, in 2015.

He is now a post-doc (Senior Research Associate) in Lancaster Environment Centre, Lancaster University, UK. From June to December 2013, he was a visiting PhD student in Geography and Environment, University of Southampton, UK. He was the recipient of the Excellent Master Dissertation Award and the Excellent Graduates in Heilongjiang Province, China, in 2012. He was awarded the hyper-competitive Hong Kong PhD Fellowship to support his three-year PhD study. His current research interests focus on remote sensing image analysis and geostatistics. He has published over 30 peer-reviewed articles in international journals such as *Remote Sensing of Environment*, *IEEE Transactions on Geoscience and Remote Sensing* and *ISPRS Journal of Photogrammetry and Remote Sensing*. He serves as a reviewer for most of the international journals in remote sensing.

Wenzhong Shi obtained the PhD degree from University of Osnabrück in Vechta, Germany, in 1994.

He is a Chair Professor in GIS and remote sensing, and the Head of Department of Land Surveying and Geo-Informatics, The Hong Kong Polytechnic University. His current research interests include GIS and remote sensing, uncertainty and spatial data quality control, image processing for high resolution satellite images. He has published over 130 SCI papers and 10 books. Prof. Shi received the State Natural Science Award from the State Council of China in 2007 and The Wang Zhizhuo Award from International Society for Photogrammetry and Remote Sensing in 2012.

Peter M. Atkinson received the BSc degree in Geography from the University of Nottingham in 1986 and the PhD degree from the University of Sheffield (NERC CASE award with Rothamsted Experimental Station) in 1990. More recently, he received the MBA degree from the University of Southampton in 2012.

He is Dean of the Faculty of Science and Technology at Lancaster University. He is also Visiting Professor at University Southampton and Queen's University Belfast, UK. The main focus of his research is in remote sensing, geographical information science and spatial (and space-time) statistics applied to a range of environmental science and socio-economic problems. He has published over 200 peer-reviewed articles in international scientific journals and around 50 refereed book chapters. He is Associate Editor for *Computers and Geosciences* and sits on the editorial boards of several further journals including *Geographical Analysis*, *Spatial Statistics*, the *International Journal of Applied Earth Observation and Geoinformation*, and *Environmental Informatics*. He sits on various international scientific committees.

Qi Wei (S'13) received a PhD degree in signal, image, acoustics and optimization (SIAO) from National Polytechnic Institute of Toulouse (INPT), University of Toulouse, France in 2015 and a BSc degree in electrical engineering from Beihang University (BUAA), Beijing, China in 2010. He is currently a Research Associate in the Department of Engineering at University of Cambridge, UK. He His doctorate dissertation about multi-band image fusion was rated as one of the best doctoral theses in 2015 at University of Toulouse. From February to August of 2012, he was an exchange master student with the Signal Processing and Communications Group in the Department of Signal Theory and Communications (TSC), Universitat Politècnica de Catalunya (UPC), Barcelona, Spain. His research has been focused on Bayesian estimation in statistical signal processing, especially on inverse problems in image processing. He has served as a reviewer for the *IEEE Journal of Selected Topics in Signal Processing*, *IEEE Transactions on Image Processing*, *IEEE Transactions on Geoscience and Remote Sensing*, and several conferences.